IEICE TRANSACTIONS

on Fundamentals of Electronics, Communications and Computer Sciences

DOI:10.1587/transfun.2024EAP1046

Publicized:2024/08/27

A PUBLICATION OF THE ENGINEERING SCIENCES SOCIETY

The Institute of Electronics, Information and Communication Engineers

Kikai-Shinko-Kaikan Bldg., 5-8, Shibakoen 3 chome, Minato-ku, TOKYO, 105-0011 JAPAN

PAPER

Analysis of superstable phenomena generated by piecewise-constant chaotic spiking oscillator with state-dependent switching

Yusuke MATSUOKA[†], ***Member***

SUMMARY This paper analyzes the superstable periodic orbits (SSPOs) generated by a piecewise-constant chaotic spiking oscillator. For this oscillator, the oscillation and reset of states are repeated, which generates chaos and SSPOs. A one-dimensional return map described by the dynamics is theoretically derived. This map has discontinuous points. A theoretical analysis of border-collision bifurcations is performed to clarify the regions of the SSPOs in the parameter space.

key words: *Bifurcation phenomenon, Superstable periodic orbit, Border-collision bifurcation, Chaotic spiking oscillator*

1. Introduction

Chaotic phenomena have been studied for nonlinear problems and chaos and related bifurcations have been extensively studied for various chaotic circuits [1]-[4]. Chaos appears in encryption [5], communication using matched filters [6], and the control of permanent-magnet synchronous generators [7]. The analysis of chaotic phenomena is thus important for engineering applications.

This paper analyzes a piecewise-constant chaotic spiking oscillator (PWCCSO), which is a chaotic circuit. The dynamics of the PWCCSO considered in this paper are as follows. Two state variables oscillate as time evolves. If one state reaches a threshold level, a spike is output and the state is instantaneously reset to a base level. The oscillation and reset of states are repeated. It is assumed that the base level depends on the value of another state (i.e., state-dependent switching is assumed). The PWCCSO produces chaos, periodic orbits, and superstable periodic orbits (SSPOs). We confirm the basic phenomena using numerical simulations and derive a one-dimensional (1D) return map that describes the dynamics to analyze the generated phenomena. The PWCCSO has a piecewise-constant vector field and a piecewise-linear trajectory. Therefore, the derived 1D return map can be described by explicit equations, making the theoretical analysis relatively simple.

Based on the 1D return map, we consider the generated phenomena in the parameter space. In particular, the 1D return map generates SSPOs with various periods when a certain parameter condition is assumed. Border-collision bifurcations (BCBs) are generated for various parameter values because the 1D return map is piecewise-linear and has discontinuous points. We calculate the bifurcation parameter values at which the BCBs occur and theoretically obtain the regions of the SSPO periods in the parameter space. A period-increment bifurcation (PIB) scenario is observed for the PWCCSO. PIBs related to basic PIBs appear. We theoretically show that the bifurcations are alternately generated.

The novelty and significance of this paper are as follows. The 1D return map of the PWCCSO is nonlinear and has discontinuous points. It is known that non-smooth 1D return maps produce different bifurcation phenomena than those produced by smooth maps [8]-[11]. Tramontana et al. [12] studied a piecewise-linear map with discontinuous points derived from a financial market dynamics model. The maps studied in [8]-[11] are mainly 1D maps consisting of two lines. The shapes of the maps in [8] and [11] have two straight lines and a discontinuity between them. The map in [9] has two lines with negative and positive slopes. A conditional analysis was conducted in [10] for various line shapes. The present study derives a 1D map that comprises four straight lines and mainly examines the dynamics of the SSPO on three lines, which have a more intricate shape than that of those in [8]-[10]. In [11], models consisting of three lines were also analyzed, but the focus was on trajectories consisting of two lines and it was stated that it is difficult to fully analyze regions where the trajectory consists of three lines.

As previously stated in [8], piecewise linear maps with a discontinuity point can result in the coexistence (bistability) of stable periodic orbits with different periods for the same parameters and different initial values. This can make the analysis challenging. The present study focuses on maps with a flat segment that causes SSPOs and where the slopes of the other segments are greater than 1. This ensures that stable periodic orbits other than SSPOs do not occur and that coexisting phenomena almost do not occur. Consequently, it is only necessary to focus on the SSPO bifurcation and a theoretical analysis can be carried out relatively easily. Furthermore, the construction of a bifurcation theory for SSPOs, such as the fold bifurcation of the superstable version, is also beneficial. It is important to note that while the maps in [8]-[11] are defined from mathematical models, the maps in the present study can potentially be included in concrete continuous dynamics models.

The PWCCSO can generate various SSPOs that are superstable for initial states but very sensitive to parameter change [13]. SSPOs appear in various applications, such as some neuron models [14]-[15], a chaos control system [16],

[†]The author is with Department of Integrated Engineering, National Institute of Technology (NIT) (Kousen), Yonago College, 4448 Hikona-cho, Yonago-shi, Tottori 683-8502, Japan

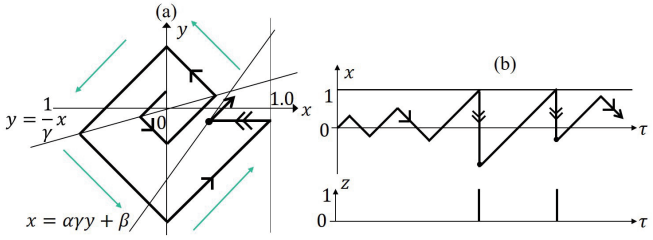

Fig. 1 Dynamics of PWCCSO. (a) Vector field and example of trajectory in phase plane and (b) example of waveform x.

an impact system [17], a switching circuit [18], an electronic oscillator [19], a model related to economics [20], and a model for natural resource harvesting policies [21]. The PWCCSO in [22] had a constant reset level and produced only chaos and divergence. The PWCCSO in the present study produces more varied phenomena. Ref. [23] derived a basic circuit model and observed basic phenomena using numerical simulations. However, they did not perform an analysis of the BCBs and did not consider the SSPO periods.

2. Basic dynamics and typical phenomena

The dynamics and reset rule of the PWCCSO considered in this paper are described by equation (1).

$$\begin{cases} \frac{dx}{d\tau} = \mathrm{sgn}(x - \gamma y) \\ \frac{dy}{d\tau} = \mathrm{sgn}(x) \end{cases} \quad \text{for } x(\tau) < 1, \qquad (1)$$
$$(x(\tau+), y(\tau+)) = (\alpha\gamma y(\tau) + \beta, y(\tau)) \quad \text{if } x(\tau) = 1,$$

where τ is dimensionless time and $x(\tau)$ and $y(\tau)$ are dimensionless variables. It is assumed that $z(\tau)$ is the output of the spike-train $z(\tau) = 1$ (or 0) for $x(\tau) = 1$ (or $x(\tau) \neq 1$). α, β, and γ are system parameters and real numbers. sgn is the signum function:

$$\mathrm{sgn}(x) = \begin{cases} 1 & \text{for } x > 0, \\ 0 & \text{for } x = 0, \\ -1 & \text{for } x < 0. \end{cases} \qquad (2)$$

The ranges of the three parameters are restricted for simplicity as follows.

$$1 < \gamma,\ 0 < \alpha < 1,\ \beta < 1 - \alpha. \qquad (3)$$

Fig. 1 (a) shows the vector field and an example of the trajectory in the phase plane. The vector field is divided into four regions (green arrows in the figure) bounded by the two lines $x - \gamma y = 0$ and $x = 0$. Therefore, for $1 < \gamma$, the trajectory that starts an initial state divergently rotates counter-clockwise around the origin. If the state x reaches the threshold $x = 1$, x is instantaneously reset to the base line $x = \alpha\gamma y + \beta$. The system again follows the differential equation and the two states divergently oscillate. α and γ correspond to the slope of the base line and β corresponds to the x-intercept. γ also corresponds to the bounded line of the vector field.

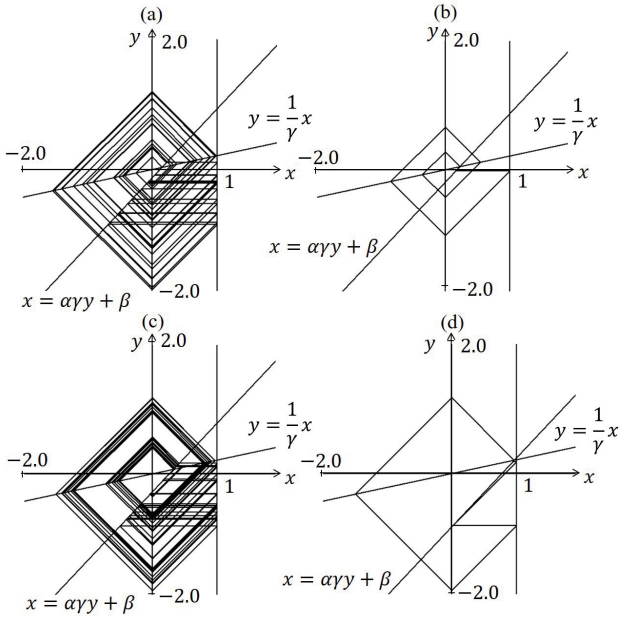

Fig. 2 Typical examples of attractors for $\gamma = 4.7$ and $\alpha = 0.2$. (a) Chaotic attractor for $\beta = 0.12$, (b) periodic attractor for $\beta = 0.18$, (c) chaotic attractor for $\beta = 0.26$, and (d) periodic attractor for $\beta = 0.77$.

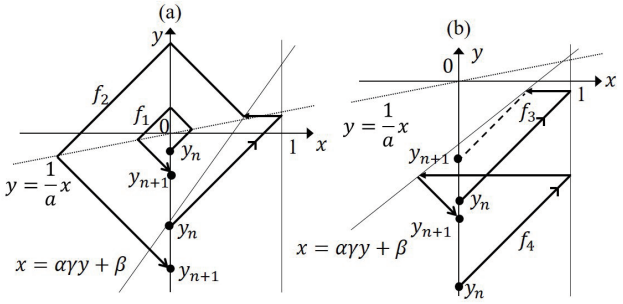

Fig. 3 Definition of 1D return map. Examples of trajectories for (a) f_1 and f_2 and (b) f_3 and f_4.

Fig. 1 (b) shows an example of the waveform of x. Because the trajectory is piecewise-linear, the 1D return map described below can be explicitly described and rigorously analyzed. Fig. 2 shows typical attractors obtained from numerical simulations. Figs. 2 (a) and (c) show chaotic attractors and Figs. 2 (b) and (d) show periodic attractors. The PWCCSO generates various phenomena.

3. Derivation of 1D return map and phenomena in parameter space

To analyze the generated phenomena, the 1D return map is defined as follows. Let y_n and y_{n+1} be the n-th and $n+1$-th points that the trajectory reaches, respectively, on the negative y axis. 1D return map F can be described by $y_{n+1} = F(y_n)$ because y_{n+1} is uniquely determined by y_n.

$$F : D \to D,\ y_{n+1} = F(y_n),\ D = \{x, y | x = 0, y < 0\}. \qquad (4)$$

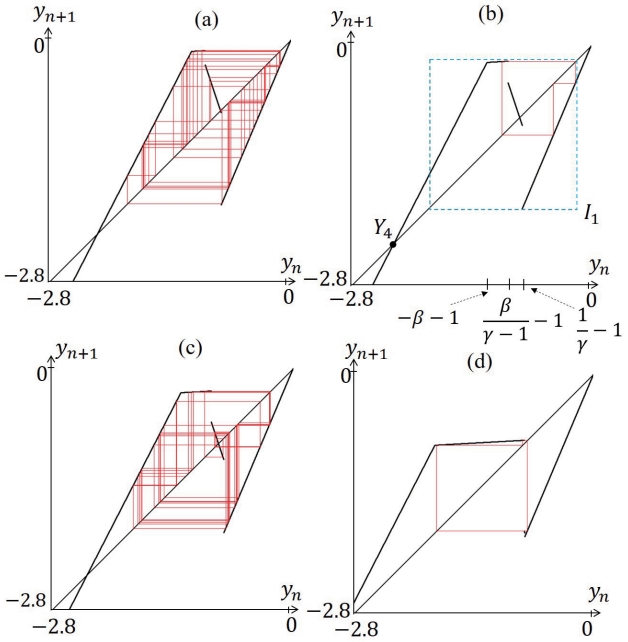

Fig. 4 Typical 1D return maps for $\gamma = 4.7$ and $\alpha = 0.2$. (a) Chaotic orbit for $\beta = 0.12$, (b) periodic orbit for $\beta = 0.18$, (c) chaotic orbit for $\beta = 0.26$, and (d) periodic orbit for $\beta = 0.77$. Parameters in these figures correspond to Fig. 2.

As shown in Fig. 3, $F(y_n)$ is calculated as four piecewise trajectories. The partial mappings are denoted $f_1(y_n)$ to $f_4(y_n)$. $f_1(y_n)$ corresponds to no reset of the trajectory and $f_2(y_n)$ to $f_4(y_n)$ correspond to resets of the trajectory. Using elementary calculation, F can be described using explicit functions as follows.

$$y_{n+1} = F(y_n)$$
$$F(y_n) = \begin{cases} f_1(y_n) & \text{for } \frac{1}{\gamma} - 1 \le y_n < 0, \\ f_2(y_n) & \text{for } \frac{\beta}{\gamma(1-\alpha)} - 1 \le y_n < \frac{1}{\gamma} - 1, \\ f_3(y_n) & \text{for } -\frac{\beta}{\gamma\alpha} - 1 \le y_n < \frac{\beta}{\gamma(1-\alpha)} - 1, \\ f_4(y_n) & \text{for } y_n < -\frac{\beta}{\gamma\alpha} - 1, \end{cases} \tag{5}$$

where $f_1(y_n) = \frac{(1+\gamma)^2}{(1-\gamma)^2} y_n$, $f_2(y_n) = \frac{(1+\gamma)}{(1-\gamma)}(1+\alpha\gamma)y_n + \frac{1+\gamma}{1-\gamma}(1+\alpha\gamma+\beta)$, $f_3(y_n) = (1-\alpha\gamma)y_n + (1-\alpha\gamma-\beta)$, and $f_4(y_n) = (1+\alpha\gamma)y_n + (1+\alpha\gamma+\beta)$.

For $f_3(y_n)$, the trajectory after a reset moves toward the bottom left. The point at which it hypothetically touches the y axis is determined as y_{n+1}. This approach is applied without loss of generality because the trajectory passes along the same line and then reaches the same point on the y axis, which does not affect the analysis. Fig. 4 shows examples of the 1D return map corresponding to the parameters in Fig. 2. We set initial state y_1 to a negative value near 0 to avoid the divergence of the trajectory. To examine the generated phenomena, we give the following definitions.

Def. 1: A point $y_p \in I$ is said to be a periodic point with period k if $y_p = F^k(y_p)$, $y_p \neq F^j(y_p)$, for $1 \le j < k$, where F^k denotes the k-fold composition of F (j does not exist for $k = 1$) and I is an invariant interval.

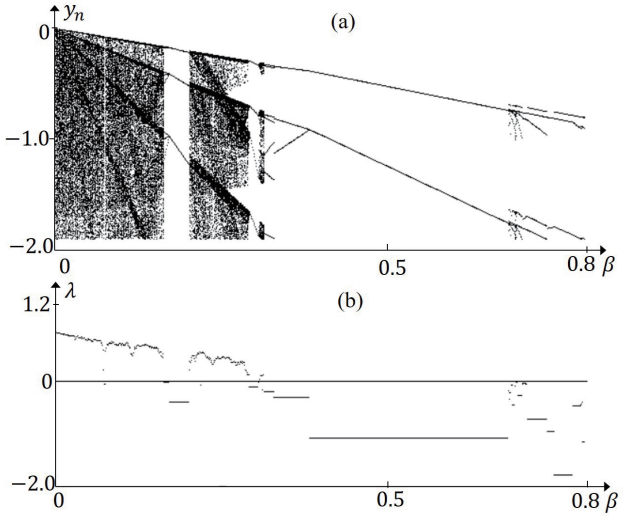

Fig. 5 Bifurcation diagram and Lyapunov exponent for $\gamma = 4.7$ and $\alpha = 0.2$.

Def. 2: Periodic points with period k are regarded as unstable, stable, and superstable for initial states $|DF^k(y_p)| > 1$, $|DF^k(y_p)| < 1$, and $|DF^k(y_p)| = 0$, respectively, where $DF \equiv \frac{d}{dy_n}F$. An orbit of superstable periodic points $\{F(y_p), \ldots, F^k(y_p)\}$ is referred to as an SSPO with period k, abbreviated as k-SSPO.

Figs. 4 (a) and (c) ((b) and (d)) show chaotic (periodic) orbits corresponding to chaotic (periodic) attractors. It should be noted that the periods of a periodic orbit and the number of points that touch the negative y axis in the periodic attractor may be different because of f_3.

A bifurcation diagram and Lyapunov exponent λ for various values of β obtained from a numerical simulation with $\gamma = 4.7$ and $\alpha = 0.2$ are shown in Fig. 5, where λ was calculated as follows.

$$\lambda_N = \frac{1}{N}\sum_{k=1}^{N}(ln|\frac{dF(y_n)}{dy_n}|), \quad \lambda = \lim_{N\to\infty}\lambda_N, \tag{6}$$

In general, the observed phenomenon tends to become more periodic as β increases. With an increase in β, the interval of $f_3(y_n)$ becomes wider and the orbit tends to become stable.

We now consider the phenomena in the parameter space. As shown in Fig. 4 (b), let Y_4 be the intersection point of the line $y_n = y_{n+1}$ and segment $f_4(y_n)$. $Y_4 = -\frac{1+\alpha\gamma+\beta}{\alpha\gamma}$ can be calculated. If $Y_4 > f_1(\frac{1}{\gamma} - 1)$ is satisfied, the orbit may diverge even if the initial state is near 0. The value of $\beta = \beta_{div}$ that satisfies $Y_4 = f_1(\frac{1}{\gamma} - 1)$ is given.

$$\beta_{div} = -\alpha(\frac{1+3\gamma}{1-\gamma}) - 1. \tag{7}$$

Fig. 6 shows the line β_{div} in β–γ space. When $\beta > \beta_{div}$, there is an invariant interval $I_1 = [f_1(\frac{1}{\gamma}-1), f_3(\frac{\beta}{\gamma(1-\alpha)}-1)]$, as shown in Fig. 4 (b), so the orbit does not diverge if the initial state is taken in the range of $Y_4 < y_1 < 0$. Hereafter, we consider that the parameter condition $\beta > \beta_{div}$ and initial

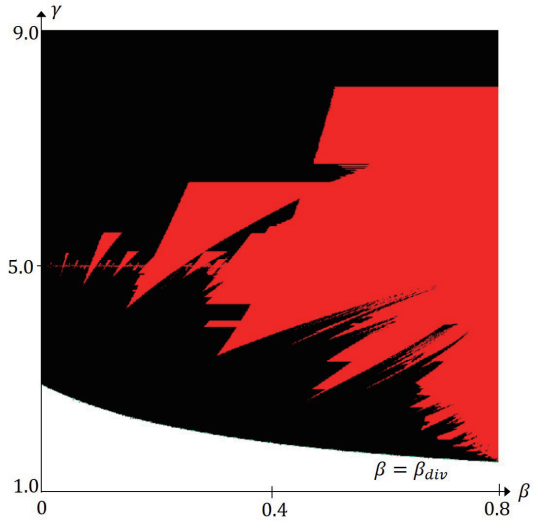

Fig. 6 Distribution of Lyapunov exponent in parameter space for $\alpha = 0.2$. Red and black regions show negative and positive Lyapunov exponents, respectively. We performed numerical simulations for parameter regions $\beta > \beta_{div}$ and $\beta < 1 - \alpha$.

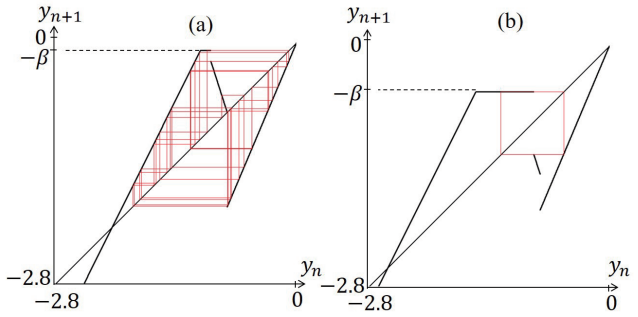

Fig. 7 Examples of 1D return map for $\gamma = 4.7$ and $\alpha = \frac{1}{\gamma}$. (a) SSPO with a long period for $\beta = 0.09$ and (b) 2-SSPO for $\beta = 0.52$.

state $Y_4 < y_1 < 0$ are satisfied. Fig. 6 shows the distribution of the Lyapunov exponent in β–γ space obtained from a numerical simulation. The red and black regions respectively show negative and positive Lyapunov exponents. In general, when γ increases, the stable region narrows and the chaotic region expands. Eventually, only the chaotic region remains.

4. Consideration of bifurcation phenomena and theoretical analysis of SSPOs

In this section, we focus on SSPOs and mainly consider the bifurcation phenomena in the parameter space. Hereafter, we set the parameter condition as follows.

$$\gamma\alpha = 1. \tag{8}$$

In this case, the equation of the 1D return map is given as

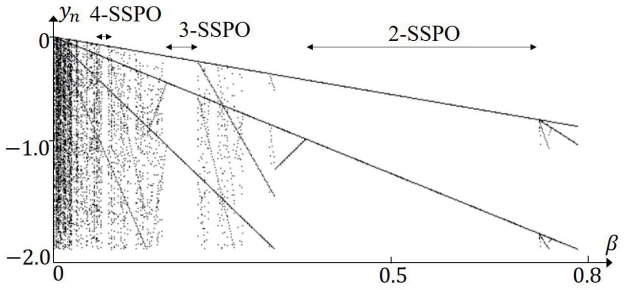

Fig. 8 Bifurcation diagram for $\gamma = 4.7$ and $\alpha = \frac{1}{\gamma}$. The almost orbit is the SSPO. SSPOs with $2, 3, 4, \ldots$ periods appear as β decreases.

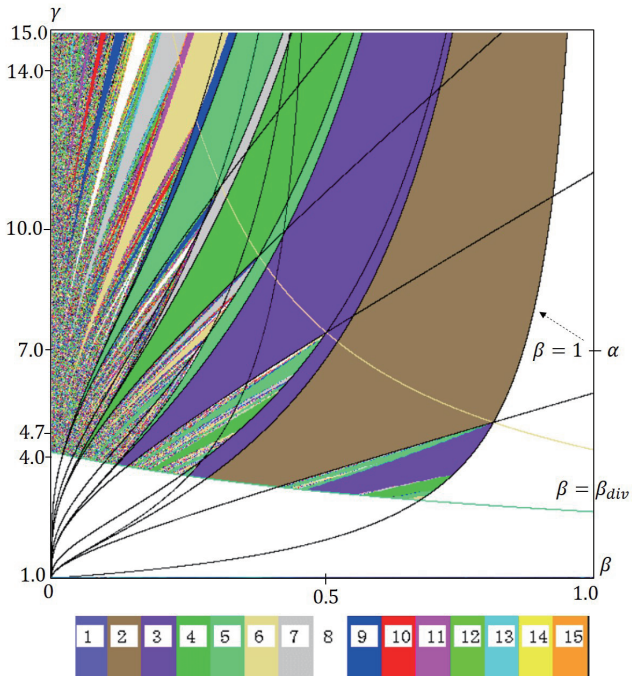

Fig. 9 Distribution of SSPO periods in parameter space for $\alpha = \frac{1}{\gamma}$. The color shows the number of SSPO periods. It should be noted that more than 15 periods are indicated by the color for 15 periods. Black lines indicate the bifurcation set of the BCB derived from the theoretical results.

$$y_{n+1} = F(y_n) = \begin{cases} b^2 y_n & \text{for } \frac{1}{\gamma} - 1 \le y_n < 0, \\ 2by_n + b(2+\beta) & \text{for } \frac{\beta}{\gamma-1} - 1 \le y_n < \frac{1}{\gamma} - 1, \\ -\beta & \text{for } -\beta - 1 \le y_n < \frac{\beta}{\gamma-1} - 1, \\ 2y_n + 2 + \beta & \text{for } y_n < -\beta - 1, \end{cases} \tag{9}$$

where $b \equiv \frac{1+\gamma}{1-\gamma}$. By the condition given in equation (8), f_3 becomes $f_3(y_n) = -\beta$ and y_{n+1} does not depend on y_n. The 1D return map has a flat segment and generates SSPOs [13].

Fig. 7 shows examples of a typical map. The orbit becomes an SSPO if it starts from the flat segment and returns. Although Fig. 7 (b) shows a 2-SSPO, the 1D return map can generate an SSPO with a very long period for certain parameter values, as shown in Fig. 7 (a). Fig. 8 shows a

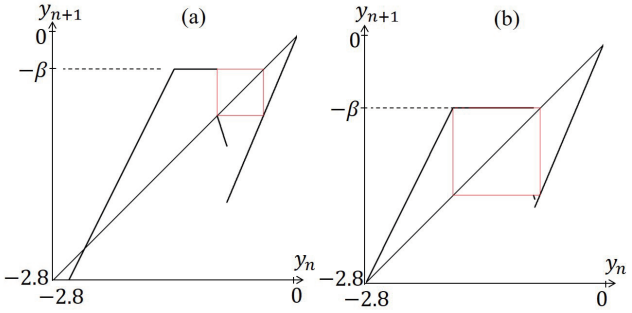

Fig. 10 1D return map related to BCB of SSPO with $m = 2$ for $\gamma = 4.7$ and $\alpha = \frac{1}{\gamma}$. Shape of 1D return map and orbit near borders (a) β_{a2} for $\beta = 0.379$, and (b) β_{b2} for $\beta = 0.728$.

bifurcation diagram. At first glance, the region around $\beta = 0$ appears chaotic; however, a very complex SSPO with a long period is generated. It should be noted that the Lyapunov exponent for this SSPO is always $\lambda = -\infty$.

Fig. 9 shows the distribution of the periods of the SSPO with $\alpha = \frac{1}{\gamma}$ in the parameter space obtained from a numerical simulation. The color indicates the number of periods. Note that more than 15 periods are indicated by the color for 15 periods. In the figure, the black lines are the theoretically calculated bifurcation set lines (see below for details). In some regions, the variation of the number of periods is very complex, whereas in other regions, the numbers of periods are very similar. We can see that the regions with $2, 3, 4, \ldots$ periods are discretely distributed as β decreases. This bifurcation scenario is called a PIB because the number of periods increases by one*. A PIB is a typical bifurcation scenario in a nonlinear map with discontinuity points. A PIB also appears in Fig. 8. As the number of periods increases, the interval of the region becomes narrow.

Hereafter, we perform a theoretical analysis of some regions of the SSPOs and clarify the bifurcation mechanism related to the SSPOs.

4.1 Theoretical analysis of SSPOs related to $f_1^{(m-1)}(f_3(y_n))$

First, we consider SSPOs that consist of only the mappings f_1 and f_3. A 2-SSPO that consists of a cycle of $f_1(f_3(y_n))$, shown in Fig. 10, is taken as an example. With a decrease in β from that in Fig. 7 (b), the periodic point on the flat segment moves to the right edge of its segment at $\beta \approx 0.379$, as shown in Fig. 10 (a). With a further decrease in β, the periodic point of the 2-SSPO on the flat segment disappears and the 2-SSPO disappears after the bifurcation. This bifurcation is called a BCB, which is a typical bifurcation generated by non-smooth return maps. The bifurcation parameter at which this BCB occurs satisfies $f_1 \circ f_3(y_n) = f_1(-\beta) = \frac{\beta}{\gamma - 1} - 1$,

*In some papers, this bifurcation scenario, in which the number of periods increases by an integer, is referred to as a period-adding bifurcation. This paper follows Avrutin and Sushko [24] and calls this scenario a PIB. It should be noted that another bifurcation scenario is referred to as a period-adding bifurcation in [24]. See [24] for details.

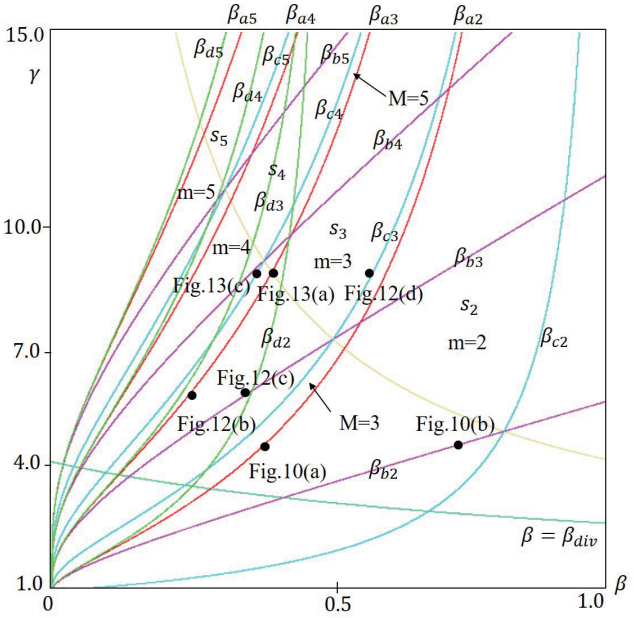

Fig. 11 Lines in BCB set in parameter space for $\alpha = \frac{1}{\gamma}$. Red, purple, light blue, and yellow-green lines show β_{am}, β_{bm}, β_{cm}, and β_{dm}, respectively. Each line is shown up to 5.

where $f_1 \circ f_3(y_n) \equiv f_1(f_3(y_n))$. After the above equation is solved for β, the border (bifurcation parameter) β_{a2} can be calculated as

$$\beta = \beta_{a2} = \frac{\gamma - 1}{1 + b^2(\gamma - 1)}. \tag{10}$$

The line β_{a2} is shown in Fig. 11. Next, as β increases for the 2-SSPO shown in Fig. 7 (b), the periodic point on the flat segment moves to the left edge of its segment near $\beta \approx 0.728$, as shown in Fig. 10 (b). With a further increase in β, the periodic point of the 2-SSPO on the flat segment disappears. This is a BCB. The 2-SSPO disappears after the bifurcation. Since the bifurcation parameter at which this BCB occurs satisfies $f_1 \circ f_3(y_n) = -\beta - 1$, after solving this equation for β, we obtain the border β_{b2}.

$$\beta = \beta_{b2} = \frac{1}{b^2 - 1}. \tag{11}$$

The line β_{b2} is shown in Fig. 11. At this bifurcation parameter, the superstable and unstable fixed points on the two-fold composition map F^2 (the periodic point with period 2) collide and disappear. This bifurcation is considered to be a superstable version of a fold BCB [20]. After the bifurcation, the orbit shows complex behavior and the period of the orbit shows a very complex change as the shape of the map determines the global behavior of the orbit. The orbits touch the segment f_4 and a complex distribution of the period is obtained for various parameter values.

Next, we consider a 3-SSPO that consists of a cycle of $f_1^2(f_3(y_n))$, as shown in Fig. 12 (a). With a decrease in β, the periodic point on the flat segment moves to the right edge of its segment and the BCB for the 3-SSPO occurs near $\beta \approx 0.25$, as shown in Fig. 12 (b). Since the bifurcation

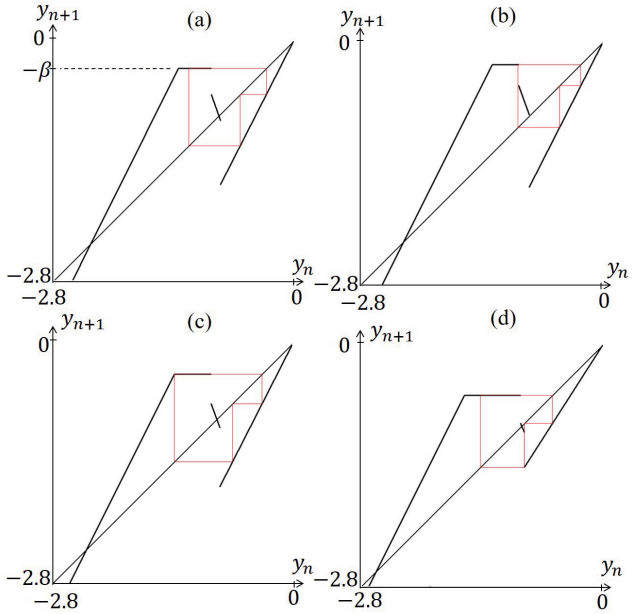

Fig. 12 1D return map related to BCB of SSPO with $m = 3$. (a) SSPO with $m = 3$ for $\beta = 0.31$. Orbits near borders (b) β_{a3} for $\beta = 0.25$, (c) β_{b3} for $\beta = 0.351$, and (d) β_{c3} for $\beta = 0.568$. $\gamma = 6.0$ and $\alpha = \frac{1}{\gamma}$ for (a)–(c). $\gamma = 9.0$ and $\alpha = \frac{1}{\gamma}$ for (d).

parameter at which this BCB occurs satisfies $f_1^2 \circ f_3(y_n) = f_1^2(-\beta) = \frac{\beta}{\gamma-1} - 1$, after solving this equation for β, we obtain the border β_{a3}.

$$\beta = \beta_{a3} = \frac{\gamma - 1}{1 + b^4(\gamma - 1)}. \tag{12}$$

With an increase in β from that in Fig. 12 (a), the periodic point on the flat segment moves to the left edge of its segment and a fold BCB occurs near $\beta \approx 0.351$, as shown in Fig. 12 (c). Since the bifurcation parameter at which this BCB occurs satisfies $f_1^2(-\beta) = -\beta - 1$, after solving this equation for β, we obtain the border β_{b3}.

$$\beta = \beta_{b3} = \frac{1}{b^4 - 1}. \tag{13}$$

This BCB is a fold BCB; therefore, the 3-SSPO disappears and the period has a complex distribution after the bifurcation (see Figs. 9 and 11).

However, different values of γ lead to different bifurcation phenomena. Fig. 12 (d) shows the 1D return map with $\gamma = 9.0$ when β increases for the 3-SSPO. In this case, before the periodic point on the flat segment moves to the left edge of its segment, one periodic point moves to the left edge of the segment f_1 near $\beta \approx 0.568$. With a further increase in β, a BCB occurs and the 3-SSPO disappears. Since the bifurcation parameter at which this BCB occurs satisfies $f_1 \circ f_3(y_n) = \frac{1}{\gamma} - 1$, after solving this equation for β, we obtain the border β_{c3}.

$$\beta = \beta_{c3} = \frac{\gamma - 1}{\gamma b^2}. \tag{14}$$

The period of the SSPO generated after this bifurcation is discussed in Subsection 4.3.

It should be noted that other bifurcations, such as flip and degenerate-flip bifurcations, do not occur because the Lyapunov exponent of the SSPO is always $-\infty$. Furthermore, the slope of the non-flat segment is greater than 1, so there are no stable periodic orbits other than the SSPO. Since the SSPO is the only orbit that starts from segment f_3 and returns, coexisting phenomena almost do not occur. We thus focus on the BCBs of SSPOs. For the 3-SSPO in Fig. 12, BCBs occur either because the periodic point on the flat segment moves to either end or the leftmost periodic point on the segment f_1 moves to the left end of its segment, as described above. Therefore, parameter region s_3, which generates a 3-SSPO that consists of a cycle of $f_1^2(f_3(y_n))$, is divided by the borders of the above BCBs (β_{a3}, β_{b3}, and β_{c3}). s_3 is described as follows.

$$s_3 = \{\gamma, \beta | \beta_{a3} < \beta < \min\{\beta_{b3}, \beta_{c3}\}\}. \tag{15}$$

Fig. 11 shows the region s_3 and the borders β_{a3}, β_{b3}, and β_{c3}. We can see that the region divided by the three BCBs (and line β_{div}) generates a 3-SSPO, as shown in Figs. 9 and 11.

Based on these considerations, the region for an m-SSPO that consists of a cycle of $f_1^{m-1}(f_3(y_n))$ can be similarly calculated.

Thereom1: Let s_m in the parameter space be the region that generates an m-SSPO that consists of a cycle of $f_1^{m-1}(f_3(y_n))$. s_m is described as follows.

$$\begin{aligned} &s_m = \{\gamma, \beta | \beta_{am} < \beta < \min\{\beta_{bm}, \beta_{cm}\}\}, \\ &\beta_{am} = \tfrac{\gamma-1}{1+b^{2(m-1)}(\gamma-1)}, \beta_{bm} = \tfrac{1}{b^{2(m-1)}-1}, \beta_{cm} = \tfrac{\gamma-1}{\gamma b^{2(m-2)}}. \end{aligned} \tag{16}$$

Proof: In addition to the 3-SSPO, three BCBs are considered. The first BCB is the border β_{am}. $f_1^{m-1} \circ f_3(y_n) = f_1^{m-1}(-\beta) = \frac{\beta}{\gamma-1} - 1$ is satisfied for β_{am}. $-b^{2(m-1)}\beta = \frac{\beta}{\gamma-1} - 1$ is true and $\beta = \beta_{am} = \frac{\gamma-1}{b^{2(m-1)}(\gamma-1)+1}$ is given. The second BCB is the border β_{bm}. $f_1^{m-1} \circ f_3(y_n) = f_1^{m-1}(-\beta) = -\beta - 1$ is satisfied for β_{bm}. $-b^{2(m-1)}\beta = -\beta - 1$ is true and $\beta = \beta_{bm} = \frac{1}{b^{2(m-1)}-1}$ is given. The third BCB is the border β_{cm}. $f_1^{m-2} \circ f_3(y_n) = f_1^{m-2}(-\beta) = \frac{1}{\gamma} - 1$ is satisfied for β_{cm}. $-b^{2(m-2)}\beta = \frac{1}{\gamma} - 1$ is true and $\beta = \beta_{cm} = \frac{\gamma-1}{\gamma b^{2(m-2)}}$ is given. However, in this case, for a 2-SSPO, $\beta_{c2} = \frac{\gamma-1}{\gamma b^0} = \frac{\gamma-1}{\gamma} = 1-\alpha$ is satisfied. This is the same parameter condition as the premise condition given in equation (3) □ .

Fig. 11 shows each border up to 5 and region s_m of the SSPO. In the figure, β_{am}, β_{bm}, and β_{cm} are shown as red, purple, and light blue lines, respectively. We can see that each region with m is divided by the corresponding borders. The BCB on β_{bm} is a fold BCB with superstability. Complex bifurcation and distribution of the periods are generated.

β_{am}, β_{bm}, and β_{cm} for each m all accumulate to the point $(0, 1)$ in the parameter space. This accumulation (or birth) of the curved line of the bifurcation set at a certain point

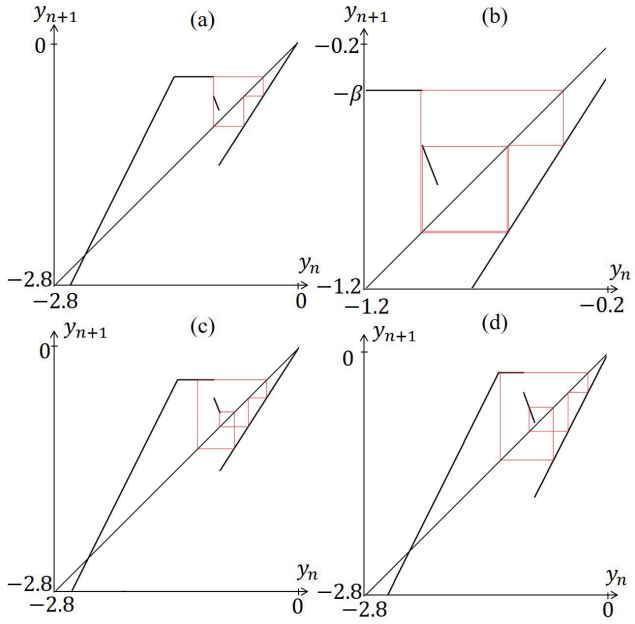

Fig. 13 1D return map related to BCB of SSPO with $M = 5$. Orbits near borders (a) β_{a3} for $\beta = 0.39$, (b) β_{a3} for $\beta = 0.389$, (c) β_{c4} for $\beta = 0.365$, and (d) β_{d3} for $\beta = 0.233$. $\gamma = 9.0$ and $\alpha = \frac{1}{\gamma}$ for (a)–(c). $\gamma = 6.0$ and $\alpha = \frac{1}{\gamma}$ for (d).

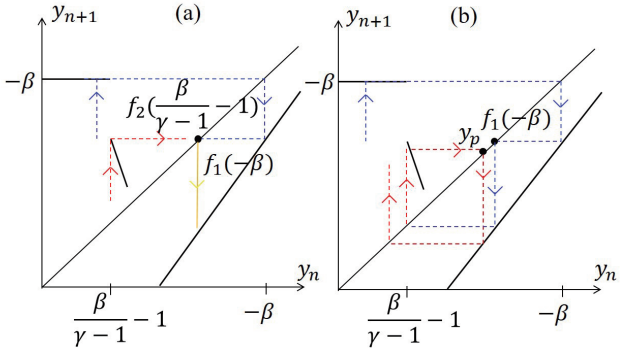

Fig. 14 Mechanism of generation of period $M = m + m - 1$. (a) Behavior of orbits $f_1 \circ f_3(y_n)$ and $f_2(\frac{\beta}{\gamma-1} - 1)$ and (b) example of 1D return map after bifurcation from period m to period M.

in the parameter space is often observed in maps where BCBs occur. In the map given in equation (9), we consider that infinite lines of the BCB set are created at the point $(0, 1)$. This bifurcation mechanism is called Big Bang bifurcation by Gardini et al. [10].

4.2 Consideration of SSPO related to BCB of β_{am}

When β decreases and exceeds the border β_{am}, a bifurcation occurs, resulting in the disappearance of an m-SSPO. Referring to Fig. 9 and Fig. 11, it can be observed that following the bifurcation, the system transitions into a narrow region with a constant period. For example, from the region $m = 2$, crossing the border β_{a2}, this system enters the region of period 3, and from the region $m = 3$, crossing the boundary β_{a3}, it enters the region of period 5. Consequently, when the system crosses the border β_{am} from the region of period m, it can be deduced that a period of $M = m + m - 1$ has occurred. This subsection analyzes the bifurcations related to β_{am} and the mechanism by which M-SSPOs occur.

We consider a decrease in β in the region s_m. The case with $m = 3$ is taken as an example. With a decrease in β from that in Fig. 13 (a), the BCB occurs at $\beta = \beta_{a3} \approx 0.38965$. After the bifurcation, the orbit becomes a 5-SSPO (see Fig. 13 (b)). In this case, a pair of periodic points appear close to each other, except for periodic point $y_n = -\beta$. The reason for this is given below.

As shown in Fig. 14 (a), the 1D return map given by equation (9) always satisfies $f_1 \circ f_3(y_n) = f_1(-\beta) = f_2(\frac{\beta}{\gamma-1} - 1)$. When the BCB is generated at $\beta = \beta_{a3}$, there is a periodic point on the left edge of the segment f_2. As β decreases, the periodic point moves to the right on the segment f_2 and a new periodic point is created and leaves from the periodic point at $f_1(-\beta)$. This is a bifurcation mechanism. Therefore, there are five periodic points after the bifurcation when $m = 3$. The generated periodic point y_p that split from $y_n = f_1(-\beta)$ in Fig. 14 (b) satisfies $y_p < f_1(-\beta)$ due to the shape of the 1D return map. Because of this, $f_1(y_p)$ is within the flat segment f_3 and an SSPO with a different period is generated. For $f_1(y_p)$ to be within the flat segment f_3, a sufficient condition is that $f_1 \circ f_2(\frac{\beta}{\gamma-1} - 1) = f_1^2(-\beta) = -b^4\beta < \frac{\beta}{\gamma-1} - 1$ is satisfied for the orbit starting from the left edge of the segment f_2. However, this is the same condition as that for a BCB with border $\beta = \beta_{a3}$ and is automatically satisfied after bifurcation. 5-SSPOs are generated from the SSPO with $m = 3$ by the bifurcation via the above mechanism.

The above discussion applies to regions with period m. That is, an SSPO with m generates bifurcation phenomena by BCBs with $\beta = \beta_{am}$ and new periodic points are created from the periodic points (except for $y_n = -\beta$). As a result, an SSPO with period $M = m + m - 1$ is generated after the bifurcation. A sufficient condition is that $f_1^{m-2} \circ f_2(\frac{\beta}{\gamma-1} - 1) = -b^{2(m-1)}\beta < \frac{\beta}{\gamma-1} - 1$ is satisfied; however, this is the same condition as that for a BCB with border $\beta = \beta_{am}$ and is automatically satisfied after bifurcation. Therefore, if β decreases in region s_m, BCBs are generated at $\beta = \beta_{am}$ and an SSPO with period $M = m+m-1$ is generated. As shown in Fig. 9, SSPOs with periods $M = 3, 5, 7$ are generated from the SSPOs with periods $m = 2, 3, 4$ when β exceeds the border β_{am}. The regions of SSPOs with period M are narrow compared with those of the SSPOs with period m.

4.3 Theoretical analysis of SSPO with period M

With a further decrease in β in the region of the SSPO with period M, two types of BCB can be generated, depending on the parameters. The case with $M = 5$ is taken as an example.

As shown in Fig. 13 (c), the first BCB is generated when the periodic point moves to the right and reaches the right edge of the segment f_2. This bifurcation parameter

satisfies $f_1^2 \circ f_3(y_n) = \frac{1}{\gamma} - 1$. After this equation is solved for β, $\beta = \frac{\gamma-1}{\gamma b^4}$ can be calculated; however, this is the same β_{c4} that is a right boundary in the region of an SSPO with $m = 4$. After this bifurcation, the 5-SSPO disappears.

As shown in Fig. 13 (d), another type of BCB is generated for other parameter values. A second BCB is generated when the periodic point on flat segment f_3 reaches the left edge of its segment. This bifurcation parameter satisfies $f_1 \circ f_2 \circ f_1^2 \circ f_3(y_n) = -\beta - 1$. After this equation is solved for β, the following can be calculated.

$$\beta = \beta_{d3} = \frac{2b^3 + 1}{2b^7 - b^3 - 1}. \tag{17}$$

After the bifurcation, the periodic points with five periods and the 5-SSPO disappear. The type of bifurcation that is generated depends on the value of the parameter γ.

Let S_5 be the parameter region of an SSPO with period $M = 5$. S_5 is divided by the borders of the above BCBs and the line β_{a3}. It can be described as follows.

$$S_5 = \{\gamma, \beta | \max\{\beta_{d3}, \beta_{c4}\} < \beta < \beta_{a3}\}. \tag{18}$$

Region S_5 and its borders are shown in Fig. 11. Whether the left border is the line β_{d3} (shown in yellow-green) or the line β_{c4} (shown in light blue) depends on the value of γ.

Based on the above description, the borders of the SSPO with period M that correspond to basic period m can be obtained.

Thereom2: Let S_M be the parameter region that generates an SSPO with period M. S_M is described as follows.

$$\begin{aligned} &S_M = \{\gamma, \beta | \max\{\beta_{dm}, \beta_{c(m+1)}\} < \beta < \beta_{am}\}, \\ &\beta_{dm} = \tfrac{2b^{2m-3}+1}{2b^{4m-5}-b^{2m-3}-1}. \end{aligned} \tag{19}$$

Proof: We consider that two BCBs can be generated as β decreases for $M = 5$. The first BCB is generated when the periodic point reaches the right edge of the segment f_2. This bifurcation parameter satisfies $f_1^{m-1} \circ f_3(y_n) = f_1^{m-1}(-\beta) = \frac{1}{\gamma} - 1$. Since $b^{2(m-1)}(-\beta) = \frac{1}{\gamma} - 1$ is satisfied, $\beta = \frac{\gamma-1}{\gamma b^{2(m-1)}}$ can be calculated. However, this result is the same as that for $\beta_{c(m+1)}$. The second BCB is generated when the periodic point on flat segment f_3 reaches the left edge of its segment. This bifurcation parameter satisfies $f_1^{m-2} \circ f_2 \circ f_1^{m-1} \circ f_3(y_n) = -\beta - 1$. By this equation, $2b^{4m-5}(-\beta) + b^{2m-3}(2 + \beta) = -\beta - 1$ is satisfied. After this equation is solved for β, $\beta = \frac{2b^{2m-3}+1}{2b^{4m-5}-b^{2m-3}-1}$ is obtained. The right border of the region is β_{am}, as discussed in Subsection 4.2 □.

The region S_M and its borders are shown in Fig. 11. In this figure, the colors of the SSPOs with periods $m = 3$ and $M = 3$ are the same and the regions unite. However, the composition of mapping f_n is different, and the regions are actually divided by the borders of the BCBs.

4.4 Parameter regions where mapping f_4 is ignored

As described in Subsections 4.1 and 4.2, a complex change in the period is generated if the orbits touch the segment f_4 through the BCB. The distribution of the period is comparatively simple if the orbits do not touch the segment f_4. We here consider the case where an invariant interval I_2 does not include the segment f_4. The following inequality is derived when specific invariant interval I_2 does not include the segment f_4, because $-\beta - 1 < b^2(\frac{1}{\gamma} - 1)$ is satisfied from $I_2 = [f_1(\frac{1}{\gamma} - 1), -\beta]$.

$$\beta > -(b^2(\frac{1}{\gamma} - 1) + 1). \tag{20}$$

The border line $\beta = -(b^2(\frac{1}{\gamma} - 1) + 1)$ (shown in yellow) is shown in Fig. 11. The condition given in equation (20) is satisfied for the region above this border. This region has bifurcations of only BCBs related to β_{am} and β_{cm} and only SSPOs with basic period m and period M derived from them. With a decrease in β, each PIB scenario for $m = 2, 3, 4 \ldots$ and $M = m + m - 1 = 3, 5, 7 \ldots$ occurs. It can be seen that they are alternately generated by the BCBs in Fig. 11. If β decreases from $\beta = 1 - \alpha$, SSPOs with $2, 3, 3, 5, 4, 7, \ldots$ periods are generated in order. Fig. 15 shows a parameter bifurcation diagram for $\gamma = 14.0$. A PIB occurs as β decreases. In the region of $\beta < -(b^2(\frac{1}{\gamma} - 1) + 1)$, the SSPO periods show a complex change. Although the interval of the PIB scenario for m becomes narrower, the PIB remains.

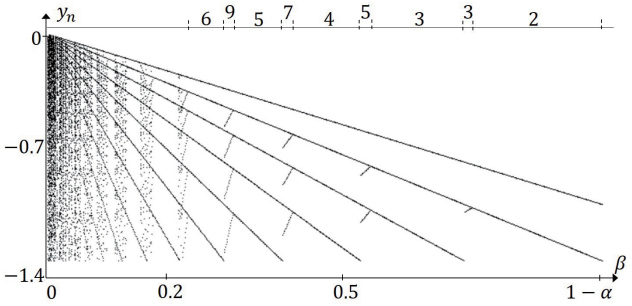

Fig. 15 Bifurcation diagram for $\gamma = 14.0$ and $\alpha = \frac{1}{\gamma}$. Numbers at top of figure indicate the numbers of SSPO periods.

5. Conclusions

This paper studied a PWCCSO with state-dependent switching. The PWCCSO generated various periodic orbits, chaos, and SSPOs. A 1D return map and an explicit equation were derived to examine phenomena related to SSPOs. The bifurcation phenomena were theoretically analyzed. We calculated the parameter conditions at which various BCBs are generated and clarified the region of SSPOs in the parameter space. We showed that there are two PIB scenarios in the parameter space and that they are alternately generated in a certain region. Future studies will consider the bifurcation analysis of a wider parameter space for chaotic and periodic phenomena, the theoretical analysis of the region that generates a complex distribution of SSPO periods, and

the analysis of an oscillator model with a reset curve and its relevance to the neuron model.

References

[1] T. Saito, "A Chaos Generator Based on a Quasi-Harmonic Oscillator", IEEE Trans. Circuit Syst., Vol. CAS-32, No. 4, pp. 320-331, 1985.

[2] C. Volos, J. Maaita, S. Vaidyanathan, V. Pham, I. Stouboulos and I. Kyprianidis, "A Novel Four-Dimensional Hyperchaotic Four-Wing System With a Saddle-Focus Equilibrium", IEEE Transactions on Circuits and Systems II, Vol. 64, No. 3, pp. 339-343, 2017.

[3] S. Euzzor, A. D. Garbo, J. M. Ginoux, F. T. Arecchi, and R. Meucci, "Implementing Poincare Sections for a Chaotic Relaxation Oscillator", IEEE Transactions on Circuits and Systems II, Vol. 67, No. 2, pp. 395-399, 2020.

[4] F. Wang, R. Wang, H. H. C. Iu, C. Liu, and T. Fernando, "A Novel Multi-Shape Chaotic Attractor and Its FPGA Implementation", IEEE Transactions on Circuits and Systems II, Vol. 66, No. 12, pp. 2062-2066, 2020.

[5] K. Cho and T. Miyano, "Chaotic Cryptography Using Augmented Lorenz Equations Aided by Quantum Key Distribution", IEEE Transactions on Circuits and Systems I, Vol. 62, No. 2, pp. 478-487, 2015.

[6] B. Rhea, R. Harrison, F. Werner, E. Perkins and R. Dean, "Approximating an Exactly Solvable Chaotic Oscillator Using a Colpitts Oscillator Circuit", IEEE Transactions on Circuits and Systems II, Vol. 68, No. 3, pp. 1028-1032, 2021.

[7] D. Zhu, R. Wang, C. Liu and J. Duan, "Synchronization of Chaotic-Oscillation Permanent Magnet Synchronous Generators Networks via Adaptive Impulsive Control", IEEE Transactions on Circuits and Systems II, Vol. 67, No. 10, pp. 2194-2198, 2020.

[8] L. Gardini and F. Tramontana, "Border collision bifurcation curves and their classification in a family of 1D discontinuous maps", Chaos, Solitons & Fractals, Vol. 44 pp. 248-259, 2011,

[9] I. Sushko and L. Gardini, "Degenerate bifurcations and Border Collisions in Piecewise Smooth 1D and 2D Maps", International Journal of Bifurcation and Chaos, Vol. 20, No. 7, pp. 2045-2070, 2010.

[10] L. Gardini, V. Avrutin, M. Schanz, A. Granados and I. Sushko, "Organizing centers in parameter space of discontinuous 1D maps. The case of increasing/decreasing branches", ESAIM: Proceedings, Vol. 36, pp. 106-120, April 2012.

[11] M. R. Jeffrey and S. Webber, "The hidden unstable orbits of maps with gaps", Proceedings of the Royal Society A: Mathematical, Physical and Engineering Sciences, Vol. 476, 2020.

[12] F. Tramontana, F. Westerhoff and L. Gardini, "One-dimensional maps with two discontinuity points and three linear branches: mathematical lessons for understanding the dynamics of financial markets", Decisions in Economics and Finance, vol. 37, pp. 27-51, 2014.

[13] Y. Matsuoka, "Robustness and an application of a one-dimensional window-map based on rotation dynamics", Nonlinear Theory and Its Applications, IEICE, vol. 3, no. 4, pp. 533-545, 2012.

[14] G. S. Medvedev, "Reduction of a model of an excitable cell to a one-dimensional map", Physica D: Nonlinear Phenomena, vol. 202, no. 1-2, pp. 37-59, 2005.

[15] S. Coombes and A. H. Osbaldestin, "Period-adding bifurcations and chaos in a periodically stimulated excitable neural relaxation oscillator", Phys. Rev. E62, no. 3, 2000.

[16] C. Wagner and R. Stoop, "Renormalization Approach to Optimal Limiter Control in 1D Chaotic Systems", J. Statistical Physics, vol. 106, pp. 97-107, 2002.

[17] H. Asahara, J. Hosokawa, K. Aihara, S. Banerjee and T. Kousaka, Almost Super Stable Periodic Orbit in an Electric Impact Oscillator, International Symposium on Nonlinear Theory and its Applications, pp. 22-26, 2012.

[18] T. Kabe, S. Parui, H. Torikai, S. Banerjee and T. Saito, "Analysis of Current Mode Controlled DC-DC Converters through Piecewise Linear Models", IEICE Trans. Fundamentals, vol. E90-A, no. 2, pp. 448-456, 2007.

[19] Y. Matsuoka and T. Saito, "Rich Superstable Phenomena in a Piecewise Constant Nonautonomous Circuit with Impulsive Switching", IEICE Trans. Fundamentals, vol. E89-A, no. 10, pp. 2767-2774, 2006.

[20] I. Sushko, L. Gardini and K. Matsuyama, "Superstable credit cycles and U-sequence", Chaos: Solitons and Fractals, Vol. 59, pp. 13-27, 2014.

[21] E. Liz and C. Lois-Prados, "Dynamics and bifurcations of a family of piecewise smooth maps arising in population models with threshold harvesting", Chaos: An Interdisciplinary Journal of Nonlinear Science, vol. 30, 073108, 2020.

[22] Y. Matsuoka and T. Saito, "A simple chaotic spiking oscillator having piecewise constant characteristics", IEICE Transactions on Fundamentals of Electronics, Communications and Computer Sciences, Vol., E89-A, No. 9, pp. 2437-2440, 2006.

[23] G. Miyamoto and Y. Matsuoka, "Piecewise Constant Chaotic Spiking Circuit with state-dependent switch", The 35th Workshop on Circuits and Systems, A5-1, 2022 (in japanese).

[24] V. Avrutin and I. Sushko, "A Gallery of Bifurcation Scenarios in Piecewise Smooth 1D Maps", Global Analysis of Dynamic Models in Economics and Finance, pp. 369-395, 2012.

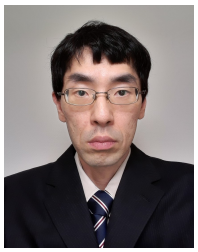

Yusuke Matsuoka received B.E., M.E. and D.E. degrees in electrical engineering from Hosei University, Tokyo, Japan, in 2004, 2006 and 2009, respectively. He is currently an associate professor at the Department of Integrated Engineering, National Institute of Technology (Kousen), Yonago College. His research interests are in chaos and bifurcation, artificial neuron models and switched dynamical systems.